PNAS

www.pnas.org

Supplementary Information for **Early life of Neanderthals**

Alessia Nava, Federico Lugli, Matteo Romandini, Federica Badino, David Evans, Angela H. Helbling, Gregorio Oxilia, Simona Arrighi, Eugenio Bortolini, Davide Delpiano, Rossella Duches, Carla Figus, Alessandra Livraghi, Giulia Marciani, Sara Silvestrini, Anna Cipriani, Tommaso Giovanardi, Roberta Pini, Claudio Tuniz, Federico Bernardini, Irene Dori, Alfredo Coppa, Emanuela Cristiani, Christopher Dean, Luca Bondioli, Marco Peresani, Wolfgang Müller, Stefano Benazzi

To whom correspondence may be addressed. Email: alessia.nava@uniroma1.it; federico.lugli6@unibo.it; marco.peresani@unife.it; w.muller@em.uni-frankfurt.de; stefano.benazzi@unibo.it

This PDF file includes:

      Supplementary text S1 to S4
      Figures S1 to S13
      Tables S1 to S3
      Legends for Datasets S1 to S3
      SI References

Other supplementary materials for this manuscript include the following:

      Datasets S1 to S3

SUPPLEMENTARY INFORMATION TEXT S1: DENTAL MORPHOLOGY

The deciduous dental sample here investigated consists of three Neanderthals and one Upper Paleolithic modern humans (UPMH) specimen.

Fig. S2 reports the surface rendering of the four teeth from high resolution microtomographic volumes, segmented with Avizo 9.2 (Thermo Fisher Scientific). High-resolution micro-CT images of Fumane 1 and 2 were obtained with a Skyscan 1172 microtomographic system using isometric voxels of 11.98 µm (Fumane 1 and Fumane 2) (see Benazzi et al (1) for details). High-resolution micro-CT images of Nadale 1 and Riparo Broion 1 were acquired with the Xalt micro-CT scanner using isometric voxels of 18.4 µm (see Arnaud et al (2) for details).

The Neanderthal specimen Nadale 1 is a lower right first deciduous molar (Fig. S1a), whose morphological description and morphometric analysis were provided by Arnaud et al (2). The taxonomical assessment of the Neanderthal tooth Fumane 1, a lower left second deciduous molar (Fig. S1b), was confirmed by metric data and non-metric dental traits (1), while the attribution of Fumane 2, an upper right lateral deciduous incisor (Fig. S1d), to modern human was based on mitochondrial DNA (3).

Riparo Broion 1 is an exfoliated upper right deciduous canine (Fig. S1c), heavily worn, with about one-fourth of the root preserved, which suggests an age at exfoliation at about 11-12 years based on recent human standards (4). The tooth is characterized by a stocky crown, bulging buccally, and a distolingual projection of a lingual cervical eminence, ultimately producing an asymmetrical outline. Overall our data concur to align Riparo Broion 1 to Neanderthals.

Overall, considering the paucity of European human remains dating to the Middle to Upper Paleolithic transition, the dental sample here investigated represents a unique exception for 1) its provenance from a restricted region of northeast Italy, ultimately removing the geographical variable as a potential confounding factor for chemical/isotopic patterns, 2) being represented by deciduous teeth, thus allowing to evaluate diet and mobility during early infancy, 3) the presence of both late Neanderthal specimens (Fumane 1 and Riparo Broion 1) and one of the earliest modern humans in

61   Europe (Fumane 2), thus providing a unique opportunity to compare subsistence

62   strategies between the two human groups around the time of Neanderthal demise.

63

SUPPLEMENTARY INFORMATION TEXT S2: ARCHAEOLOGICAL AND

65 **PALEOENVIRONMENTAL CONTEXTS**

66

67 <u>Nadale 1</u>

68 De Nadale Cave is a small cavity located 130m a.s.l. in the middle of the Berici Hills.

69 Research at De Nadale Cave started in 2013 when a first excavation campaign led to the

70 discovery of a cave entrance after the removal of reworked sediments. Later, six

71 campaigns were carried out between 2014 and 2017 in order to investigate the deposits

72 preserved in the cave entrance and the back (5). The excavations exposed a stratigraphic

73 sequence which includes a single anthropic layer (unit 7) embedded between two sterile

74 layers (units 6 and 8) partly disturbed by some badger's dens along the cave walls. Unit 8

75 lays on the carbonate sandstone bedrock. Besides these disturbances, unit 7 is well

76 preserved and extends into the cavity. It yielded thousands of osteological materials,

77 lithic implements, and the Neanderthal deciduous tooth (2). A molar of a large-sized

78 ungulate was U/Th dated to 70,200±1,000/900 years as a minimum age (5) placing the

79 human occupation to an initial phase of the MIS 4. The zooarchaeological assemblage is

80 largely ascribable to human activity (6). Neanderthals hunted and exploited mainly three

81 taxa: the red deer (*Cervus elaphus*), the giant deer (*Megaloceros giganteus*) and bovids

82 (*Bison priscus* and *Bos primigenius*) (6, 7), in association with other taxa consistent with

83 the paleoclimatic and paleoenvironmental reconstruction based on the small mammal

84 association, where the prominence of *Microtus arvalis* identifies a cold climatic phase

85 and correlates to a landscape dominated by open woodlands and meadows (8). A large

86 amount of anthropic traces is observed on the ungulate remains, ascribable to different

87 stages of the butchery process and to the fragmentation of the bones for marrow

88 extraction. Burnt bone fragments and charcoal accumulations have been likely related to

89 residual fire-places (6). Lithic industry from of De Nadale differentiates technologically

90 and typologically from the Mousterian elsewhere in the region, especially with regard to

91 the core reduction methods and the types of flakes and retouched tools. These are

92 represented from several scrapers with stepped-scaled invasive retouches and make the

93 De Nadale industry comparable to Quina assemblages in Italy and Western Europe (5).

94 De Nadale peculiarity is also enhanced by the high number of bone retouchers (9).

95 Research at the De Nadale Cave is coordinated by the University of Ferrara (M.P.) in the

96 framework of a project supported by the Ministry of Culture – "SABAP per le province

97 di Verona, Rovigo e Vicenza" and the Zovencedo Municipality, financed by the H.

98 Obermaier Society (2015), local private companies (R.A.A.S.M., Saf and Lattebusche),

99 and local promoters.

100

101 <u>Fumane 1 and 2</u>

102 Grotta di Fumane (Fumane Cave) is a cave positioned at the western fringe of the Lessini

103 plateau in the Venetian Pre-Alps. The site preserves a finely layered late Middle and early

104 Upper Paleolithic sequence with evidence of cultural change related to the demise of

105 Neanderthals and the arrival of the first Anatomically Modern Humans (3, 10-12). Teeth

106 Fumane 1 and Fumane 2 were found in Middle Paleolithic unit A11 and Upper

107 Paleolithic unit A2 associated to Mousterian and Aurignacian cultures respectively.

108 Of the late Mousterian layers, unit A11 is a stratigraphic complex composed of an

109 ensemble of thin levels with hearths that was surveyed in different years at the eastern

110 entrance of the cave over a total area of 10 sqm. The chronometric position of A11 is

111 provided by only one U/Th date to 49,000±7,000 years for level A11a, given unreliability

112 to the radiocarbon dataset currently available (13) but see (14). New radiocarbon

113 measurements are in progress. Paleoecological indexes calculated on the composition of

114 the micromammal assemblage point for a temperate and relatively moist period related to

115 an interstadial before HE5 (15), in a landscape dominated from open-woodland

116 formations in accordance with the previous indications based on the zooarchaeological

117 assemblage. Cervids (red deer, giant deer and roe deer) largely prevail on bovids and

118 caprids (ibex and chamois) and other mammal species (16). No taphonomic analyses

119 have still been conducted to confirm the anthropogenic nature of the accumulation of the

120 animal bone remains. Lithic artifacts belong to the Levallois Mousterian. The use of this

121 technology is recorded by high number of flakes, cores and by-products shaped into

122 retouched tools like single and double scrapers, also transverse or convergent and few

123 points and denticulates (11).

124 Aurignacian layer A2 records an abrupt change in material culture represented from lithic

125 and bone industry (10, 17, 18), beads made of marine shells and bone (10, 19), use of red

126 mineral pigment (20). Bone and cultural remains have been found scattered on a

127 paleoliving floor with fire-places, toss zones and intentionally disposed stones (21). A

128 revised chronology of the Mid-Upper Paleolithic sequence (14) has shown that the start

129 and the end of level A2 date respectively to 41,900-40,200 cal BP and 40,300-39,400 cal

130 BP at the largest confidence interval. Macro- and micro-faunal remains show an

131 association between forest fauna and cold and open habitat species typical of the alpine

132 grassland steppe above the tree line in a context of climatic cooling (15, 22, 23). Hunting

133 was mostly targeted adult individuals of ibex, chamois and bison and occurred

134 seasonally, from summer to fall (22, 24).

135 Research at Fumane is coordinated by University of Ferrara (M.P.) in the framework of a

136 project supported by the Ministry of Culture – "SABAP per le province di Verona,

137 Rovigo e Vicenza", public institutions (Lessinia Mountain Community - Regional

138 Natural Park, Fumane Municipality, BIMAdige, SERIT) and by private institutions,

139 associations and companies. Research campaigns 2017 and 2019 have received funding

140 from the European Research Council (ERC) under the European Union's Horizon 2020

141 research and innovation programme (grant agreement No 724046 – SUCCESS,

142 http://www.erc-success.eu).

143 Riparo Broion 1

144 The Berici Mounts are a carbonatic karst plateau at low altitude at the southern fringe of

145 the Venetian Pre-Alps in the Alpine foreland. This is a large alluvial plain that was

146 formed initially during the Middle and Late Pleistocene by a number of major rivers,

147 including the Po, the Adige and those of the Friulian-Venetian plain. The western zone of

148 the Berici is a gentle landscape which conjoins to the alluvial plain. Conversely, along its

149 eastern slope the plateau connects abruptly to the alluvial plain. Here, caves and

150 rockshelters have been archaeologically investigated since the XIX century up to present

151 days by teams from the University of Ferrara. Of these cavities, Riparo del Broion is a

flagship site for the late Middle and early Upper Paleolithic in this area. It is situated at 135m a.s.l. at the base of a steep cliff of Mount Brosimo (327 m a.s.l.) along a terraced slope for cultivation during recent historical times. The shelter is 10m long, 6m deep and 17m high and originated from rock collapse along a major ENE-WSW oriented fault that developed from thermoclastic processes and chemical dissolution comparably to other cavities in the area (25, 26). Two additional Paleolithic cavities were investigated on the western side of the same cliff, Grotta del Buso Doppio del Broion and Grotta del Broion (27, 28).

The sedimentary deposits of Riparo Broion were partially dismantled in historical times by shepherds with use to store hay and wood. Further damage occurred in 1984 when unauthorized excavators removed sediments from pits and trenches on a total area of 14sqm down to 2m at the deepest. Archaeological excavations were initially directed by Alberto Broglio (1998 -2008) and by two of us (M.P. and M.R.) in 2015 on a 20sqm area bounded to north and west from the rock walls. Faunal remains and Middle and Upper Paleolithic (Uluzzian, Gravettian and Epigravettian) cultural material was uncovered (29-31). The bedrock has not yet been reached. Sediments are mostly small stones and gravel with large prevalence on loams: 16 stratigraphic units planarly bedded have been identified. The lowermost (11, 9, 7 and 4) contain Mousterian artefacts, faunal remains and clearly differentiate in dark-brownish color from the other units.

The human canine was discovered in unit 11 top. This unit has been 14C dated to 48,100±3100 years BP with range from 50.000 to 45.700 years cal BP as the most likely age (31). Stone tools are too low in number to propose an attribution to one or another Mousterian cultural complex. Preliminary zooarchaeological data report a variety of herbivores such as elk, red deer, roe deer, megaceros, wild boar, auroch/bison, a few goats and horses, and common beaver associated sparse remains of fish and freshwater shells. This association reflects the presence of a patchy environmental context, with closed to open-spaced forests, Alpine grasslands and pioneer vegetation complemented by humid-marshy environments and low-energy water courses, wet meadows and shallow lacustrine basins.

Paleoenvironmental contexts

The paleoenvironmental contexts during the time intervals of the teeth recovered at the sites of Nadale, Fumane cave and Riparo Broion (~ 70, 50 and 40 ka) can be inferred on the basis of two high-resolution paleoecologically records from NE-Italy: Lake Fimon (Berici Hills) and Palughetto basin (Cansiglio Plateau, eastern Venetian Pre-Alps). Pie charts presented in Fig. S3 show the relative abundances of different vegetation types at 5000 years' time-slice intervals. Pollen % are calculated based on the sum of terrestrial taxa and represent mean values. Pollen taxa are grouped according to their ecology and climatic preferences. Eurythermic conifers (EC): sum of Pinus and Juniperus; Temperate forest (TF): sum of deciduous Quercus, Alnus glutinosa type, Fagus, Acer, Corylus, Carpinus, Fraxinus, Ulmus, Tilia and Salix; Xerophytic steppe (XS): sum of Artemisia and Chenopodiaceae. Other herbs: sum of terrestrial herbs, Chenopodiaceae excluded. Original pollen data used for % calculation for the Palughetto basin are from (32).

On a long-term scale, the paleoecological record from Lake Fimon points to persistent afforestation throughout the Early to Middle Würm in the Berici Hills (i.e., Nadale, Fumane and Riparo Broion sites). Moderate forest withdrawals occurred during Greenland stadials (GSs), possibly enhanced during GSs hosting Heinrich Events (HEs) (33).

Between 75 and 70 ka, at the end of the second post-Eemian interstadial, the landscape was dominated by a mosaic of boreal forests with eurytermic conifers (46%) and

subordinated temperate taxa (10%). Open environments are identified by pollen of herbaceous taxa and steppe/desert forbes-shrubs (23%).

During the 50-45 ka and 45-40 ka time-slices, steppic communities further increase (7-8%) as a result of enhanced dry/cold conditions during Greenland stadials (GSs). Pollen of eurythermic conifers sum up to 37-38%. Temperate trees, notably Tilia, persisted in very low percentages (4%) up to ~40 ka (34).

SUPPLEMENTARY INFORMATION TEXT S3: TOWARDS A CONCEPTUAL MODEL FOR Sr/Ca AND Ba/Ca BEHAVIOR IN HUMAN INFANTS: THEORETICAL FRAMEWORK AND EMPIRICAL EVIDENCE FROM CONTEMPORANEOUS INFANTS WITH KNOWN FOOD INTAKE

Strontium and barium are non-bioessential trace elements with no major metabolic functions in the human body. Strontium and Ba mimic Ca, given their coherent behavior as alkaline earth elements with respect to their divalent charge, but are characterized by larger ionic radii (Sr: 1.18, Ba: 1.35, Ca: 1.00 Å (10^{-10} m); (35). Overall, they both follow the Ca metabolism but due to their larger ionic size are discriminated against in the gastrointestinal tract (GIT) (36, 37). Given the larger size, Ba is even more strongly discriminated against relative to Sr (37, 38). Similarly, kidneys tend to excrete Sr and Ba more rapidly compared to Ca (39). From plasma, Sr, Ba and Ca are mainly fixed in bones and teeth with a likely further bias in favor of Ca (39, 40). Taken together, these factors cause Ca-normalized concentrations of Sr and Ba in skeletal tissues to be lower than those of the diet, a process known as 'biopurification' (36). Burton and Wright (41) demonstrated that Sr/Ca of bones is approximately 5 times lower than the respective Sr/Ca value of the diet. Such evidence has been also demonstrated empirically by many studies (36-38, 42, 43). These pioneering studies also emphasized that Sr/Ca and Ba/Ca might be used as tools for paleodiet and trophic chain reconstruction (36).

Interestingly, significant GIT discrimination of Sr and Ba over Ca ions progressively increases during human growth and becomes significant at around one year of age (44, 45). This hints that both the Sr/Ca and Ba/Ca ratios of infant plasma (<1 year) should be closer to the value of their respective dietary inputs (46). Indeed, Lough et al (46) demonstrated that the relative ratio between body Sr/Ca and dietary Sr/Ca for an infant is ~0.90. Hence, for example, in breast-fed infants, the Sr/Ca of their blood plasma should reflect the Sr/Ca of the consumed breastmilk. Studies of elemental transport in humans have shown that Ca is actively transported (47), resulting in lower Sr/Ca ratios in both umbilical cord sera and breastmilk than in mother sera due to the larger size of Sr ions compared to Ca ions. Yet, empirical evidence indicates that mammary gland discrimination for Sr (2.5-fold) is higher than placenta (1.7-fold), yielding average

247   breastmilk Sr/Ca values lower than umbilical cord (fetal) values (48). Crucially, fetal

248   blood chemistry is recorded in prenatal dental enamel and breastmilk consumption in

249   postnatal enamel and can be reconstructed via high-spatial resolution chemical analysis of

250   teeth (49, 50). Thus, higher Sr/Ca signals in prenatal domains followed by lower

251   postnatal Sr/Ca indicate breastmilk consumption (see Fig. S4). This has been previously

252   shown by the Sr/Ca distribution in teeth (50, 51), but also in elemental analyses of sera

253   samples. Krachler et al. (52) showed that Sr/Ca levels are two times higher in umbilical

254   cord sera than in breast-fed infant sera. On the other hand, due to the nominal lower

255   trophic level of herbivores, their milk has higher Sr/Ca than human milk. Hence, when a

256   child is fed through formula (largely based on cow milk), a Sr/Ca increase in the

257   postnatal enamel is expected (Fig. S4).

258   Indeed, Krachler et al. (52) reported high Sr/Ca values in formula-fed infant sera.

259   Moreover, a compilation of published Sr/Ca data of geographically dispersed human and

260   bovine/caprine milks (Fig. S5 and references in caption) indicates that human breastmilk

261   has a rather homogeneous Sr/Ca ratio of $\sim 0.1 \pm 0.01 \ast 10^{-3}$, 4 times lower than non-human

262   milk and formula ($\sim 0.39 \pm 0.15 \ast 10^{-3}$).

263   From all these inferences, the Sr/Ca ratio of both breast-fed and formula-fed infants can

264   be modelled relative to an initial Sr/Ca mother diet, set equal to 1 (Tab. S2 and Fig. S4).

265   With the introduction of transitional food in the infant diet, a change in Sr/Ca values is

266   also expected. If the child was initially breast-fed, one should predict an increase of the

267   Sr/Ca ratio during transitional feeding, because both meat and especially vegetables

268   retain higher Sr/Ca than breastmilk (see e.g. 53). In general, an increased Sr/Ca signal

269   from transitional foods is also expected for formula-fed babies. However, due to the

270   compositional variability of some formulas (e.g. soy-based) and non-human milk, a

271   decrease of the Sr/Ca ratio may occur if a highly-biopurified food (e.g. close to human

272   milk) is used for initial weaning.

273   Contrary to strontium, a reliable interpretation of Ba/Ca data is difficult due to

274   contradictory literature and the lack of studies on Ba metabolism. Austin et al. (54)

275   suggested that the increased level of both Sr/Ca and Ba/Ca ratios in breast-fed infants

276   reflected improved Sr and Ba absorption during breastfeeding. Such an increase in Sr/Ca

is in stark contrast to any other study on breastfed children (49, 50). Similarly, Krachler et al. (55) highlighted increased levels of Ba/Ca in colostrum and breast-fed infant sera compared to umbilical cord sera (Tab. S3). However, colostrum is not a good proxy for breastmilk elemental content, being highly enriched in metals (56, 57). In fact, when compared with Sr/Ca and Ba/Ca ratios from literature, colostrum values reported in Krachler et al. (55) are about 2 times higher than other human milk samples (Figure S5). Moreover, other studies suggested that only a very limited portion of the absorbed Ba (~3%) is transferred to the breast-milk (48).

Studies of dental enamel indicate that Ba overall behaves akin to Sr (50, 53, 58, 59), decreasing with breastmilk consumption and increasing along with the introduction of transitional food. Still, Müller et al. (50) noted that Ba behavior in tooth enamel is less predictable than Sr. This observation may also relate to the high variability of Ba content in human milk, colostrum and formulas (see (55) and Fig. S5). Notably, Taylor et al. (60) pointed out that in controlled-fed rats, the consumption of cow milk leads to an increase of Ca absorption, without changing the Ba absorption. This, in turn, corroborates the idea that the relative Ba/Ca ratio in rats should decrease with a milk-based diet and increase with a non-milk diet. In the same publication, the authors reported that Ba absorption increased two-fold in young starved rats, whereas Ca absorption decreased in the same individuals, pointing towards an association of Ba/Ca with dietary stress rather than weaning transitions.

Around one year of age, both Ba/Ca and Sr/Ca gradually decrease due to the progressive increase in GIT discrimination in the infant due to a preferential absorption of Ca relative to Sr and Ba (44, 45). Taken together, we conclude that models for Sr/Ca with respect to dietary transitions in early life have a stronger theoretical basis compared to Ba.

The modern reference sample

In the following we present spatially-resolved chemical data from contemporaneous individuals with known dietary behavior to evaluate the theoretical framework presented above. To avoid the problem of retrospectively reporting breastfeeding and weaning practice (61), we selected offspring from parents who reliably took and preserved notes

307   of the feeding practice during the nursing period (explicit written consent was obtained

308   by all relevant people with legal authority). All individual data were treated in a fully

309   anonymous way and it is not possible from the present results to identify the involved

310   individuals.

311   Three deciduous teeth, representing three different nursing histories, were analyzed by

312   LA-ICPMS: an exclusively breastfed individual from Switzerland (deciduous second

313   molar dm2; MCS1), an exclusively bottle-fed individual from central Italy (deciduous

314   canine dc; MCS2 previously published as MOD2 in (50)), a mixed breast-/bottle-fed

315   individual from central Italy (deciduous canine dc; MCS3). The mothers of the three

316   infants did not travel for extended periods during the interval in which these deciduous

317   teeth were forming.

318   MCS1 is a lower deciduous second molar from an individual exclusively breastfeed until

319   the fifth month of life (154 days; Fig. S6). No supplementary food was given to the infant

320   during this period. The Sr/Ca profile analyzed parallel to the enamel-dentine junction

321   (EDJ) shows a constant decrease in the elemental ratio until ~154 days corresponding to

322   the reported period of exclusive breastfeeding. Just after the introduction of solid food

323   once a day (reported from day 155), the slope of the profile becomes gradually shallower,

324   particularly, this was coincident with the introduction of some formula milk (reported

325   from day 182). Fifteen days after cutting down breastfeeding during daytime (reported on

326   day 209) the profile begins to show a sharp increase of the Sr/Ca values. At 8.5 months of

327   life (reported on 258 days) the breastfeeding period of individual MCS1 stopped and the

328   diet continued with solid food and formula milk. The rather flat Sr/Ca signal observed in

329   the last part of the profile (after day ~340) likely reflects the effects of maturation-

330   overprint due to the thin enamel closest to the crown neck (50). The striking

331   correspondence of the independently recorded dietary transitions in MCS1 with the Sr/Ca

332   trend fully supports the use of Sr/Ca as a proxy for making nursing events. In this sense,

333   based on modelled values reported in Tab. S2, the theoretical ratio between Sr/Ca in

334   prenatal enamel and breastfeeding signal is ~0.7. In MCS1, this ratio is ~0.8, indicating a

335   remarkable correspondence between the theoretical model and the observed data. The

336   MCS1 Ba/Ca profile broadly follows the trend observed for Sr/Ca, decreasing - with

337 proportionately smaller changes in Ba levels across lifetime - from birth until ~160 days.
338 Thereafter, Ba/Ca steadily increases till day 235, steeply increases until day ~290 (9.5
339 months) to then decrease again for 25 days. Finally, Ba/Ca constantly increases to the end
340 of the crown formation. This fluctuation in the last part of the profile cannot be explained
341 by any event in the known dietary/health history of MCS1.

342 MCS2 is a deciduous canine from an exclusively formula-fed individual (Fig. S7), whose
343 results have already been partially presented in the context of enamel mineralization
344 processes as MOD2 (50). The Sr/Ca profile, run parallel to the EDJ, shows a constant
345 increase after birth until ~130 days (~4.3 months), and then it starts to decrease as a
346 consequence of the combined effects of the onset of the reported transitional period and
347 maturation overprint. The absolute values of Sr/Ca through all the postnatal period are
348 higher than $5*10^{-4}$ and thus higher than those observed in the other contemporary
349 reference individuals (Figure S4b). The model reported in Fig. S4 and Table S2 specifies
350 a ratio between prenatal enamel and formula Sr/Ca signal equal to ~2.2. In MCS2, this
351 ratio is ~1.8, corroborating the hypothesis that with formula introduction the postnatal
352 Sr/Ca should double. The Ba/Ca profile follows the same trend observed in the Sr/Ca
353 profile, increasing from birth until ~75 days (2.5 months), then remaining stable with
354 some fluctuation until ~175 days (5.8 months).

355 MCS3 is an upper deciduous canine from a mixed breast- formula-fed individual (Fig.
356 S8). This infant was exclusively breastfed for the first 30 days. After that, the mother
357 complemented the infant diet with formula milk. Mixed feeding was carried on until 4
358 months of age, at which time the mother underwent surgery. During this period of illness,
359 the mother used a breast pump to continue breastfeeding. After the surgery, the mother
360 continued to breastfeed the infant with formula milk supplements, until the onset of
361 weaning at six months.

362 The X/Ca profiles were nominally analyzed close to daily-resolution (6 µm spots vs. 10.3
363 µm/day mean enamel extension rate), well-reflecting this complex nursing history and
364 almost perfectly matching the main dietary shifts. Ba/Ca mirrors the Sr/Ca pattern,
365 decreasing during the period of exclusive breastfeeding, slightly increasing during the
366 mixed breast- bottle-feeding, and increasing further at the onset of weaning. The Ba/Ca

profile follows the main dietary shifts but with less precision than Sr/Ca. Moreover, as in MCS1, the period of exclusive breastfeeding is characterized by a sharp decrease in Ba/Ca, contrary to what expected by Austin et al. (54), that predict in their model increased levels of both Sr/Ca and Ba/Ca ratios in breast-fed infants. We note here that the small laser spot (6 µm) used during analysis resulted in lower ICPMS signals and hence overall larger analytical variability than for the other two specimens.

The fossil Late Pleistocene human dental sample

Nadale 1 - Neanderthal

In Nadale1, Sr/Ca profile slightly decreases until the end of the elemental profile, depicting a breastfeeding signal until the end of the crown formation. Unusually, Ba/Ca shows the opposite trend to Sr/Ca (Fig. S9) and appears to follow the dietary model proposed by (54), i.e. an increase in Ba/Ca. Mg/Ca is largely invariant across the whole crown, and only very minor diagenetic alteration is apparent via U peaks at the very beginning and end of the crown that have very limited correspondence in Ba/Ca and Sr/Ca.

Fumane 1 - Neanderthal

In Fumane 1, the Ba/Ca profile broadly follows that of Sr/Ca (Fig. S10), yet especially for the first ~120 days displays several pronounced, narrow peaks that correlate positively with U and negatively with Mg, respectively. These reveal localized diagenetic overprint that is far less manifested for Sr/Ca. According to our model, Sr/Ca indicates an exclusive breastfeeding signal until 115 days (4 months), followed by the first introduction of non-breastmilk food and a stronger signal visible at 200 days (6.6 months), at which point there is a steep increase in Sr/Ca that likely indicates a more important and substantial introduction of supplementary food. This profile is fully comparable to the MCS1 pattern reported above. According to (54), this individual falls outside the bounds of their model, because a decrease in Ba/Ca after birth due to exclusive breastfeeding is never detected in their data (see above for an explanation of the Ba/Ca model reported in (54)).

397 Riparo Broion 1 - Neanderthal

398 In Riparo Broion 1, the Ba/Ca profile overall varies in parallel with the Sr/Ca one (Fig.

399 S11), but also shows some prominent peaks that correlate positively with U and

400 negatively with Mg, respectively, indicating, similar to Fumane 1, that U uptake and Mg

401 loss are indicators of localized diagenetic alteration (see Figure 3 main text). Regardless

402 of diagenesis, both elemental ratios vary in the same way. According to our contemporary

403 reference sample, a decrease in the Sr/Ca ratio is a consequence of exclusive

404 breastfeeding until 160 days (5 months), after which an increase in Sr/Ca points to the

405 first introduction of non-breastmilk food. According to the Ba/Ca profile and following

406 the model in (54), this individual should have been never breastfed.

407

408 Fumane 2 - Aurignacian

409 The Ba/Ca profile of Fumane 2 follows that of Sr/Ca (Fig. S12), slightly decreasing in the

410 first month of postnatal life and then increasing in the most cervical enamel. The short

411 postnatal portion of available enamel (~55 days) precludes the chemical detection of the

412 onset of weaning but a clear breast-feeding signal is detectable after birth since Sr/Ca

413 decreases. Ba/Ca also decreases accordingly, and all is independent of diagenesis that is

414 very low. According to the Ba/Ca profile and following the model in (54), this individual

415 was breastfed for the first time at ~1 months of age.

416

SUPPLEMENTARY INFORMATION TEXT S4: ASSESSMENT OF POST-MORTEM DIAGENETIC ALTERATION OF BIOAPATITE

In order to retrieve primary in-vivo elemental and isotopic signals from fossil teeth, preferably no alteration by post-mortem diagenetic processes should have taken place. During the post-depositional history, however, bioapatite may react with soils and underground waters, which can modify the initial biogenic chemical composition. Depending on apatite crystal-size, organic content and porosity, the distinct dental tissues behave differently in a soil environment. Bone and dentine are most susceptible to diagenetic chemical overprint, in contrast to highly-mineralized enamel (62-65). Equally, the extent of chemical overprint depends on the concentration gradient between burial environment and bioapatite tissue as well as the partition coefficient for the element(s) concerned.

While alkali-earth elements (e.g. Ba, Mg and Sr) and biologically-important divalent metals (e.g. Cu, Fe and Zn) are present at mid-high concentrations (i.e. $>1 - 10^3$ µg/g) in modern bioapatite, Rare Earth Elements (REE), actinides and high-field strength elements (e.g. Hf, Th and U) have very low concentrations (lowest ng/g) in modern teeth/bones, yet are usually strongly incorporated into apatite during fossilization processes (66).

In particular, uranium as water soluble (as uranyl $(UO_2)^{2+}$) and highly mobile element is readily incorporated into bioapatite (67, 68), such that uranium in fossil bioapatite, especially in bone and dentine, often shows high concentrations ($>10s - 100s$ µg/g), whereas enamel frequently displays much lower U concentrations (e.g. (69)). Given these variations at the microscale, uranium can reveal diagenetic overprint in tandem with Mn or Al. Conversely, some bio-essential trace elements in bioapatite such as Mg may decrease post-mortem due to precipitation of diagenetic phases with lower trace metal concentrations, incipient recrystallization or leaching from the dental/bone tissue (70, 71). To monitor diagenetic alterations of our fossil dental specimens, we monitored [25]Mg, [27]Al, [55]Mn, [89]Y, [140]Ce, [166]Er, [172]Yb and [238]U signals during the LA-ICPMS analyses and found that U (and Al) were the most sensitive indicators of diagenetic alteration, while

447 commonly utilized REEs plus Y were rather insensitive in all cases as they remained at

448 detection limit even in domains with clearly elevated U and Al. As a result, REE + Y are

449 not shown here and we focus on U as main proxy for post-mortem diagenesis.

450 Scatter plots between U and the residuals of Sr, Ba or Mg variation for the diagenetically

451 most affected segments (Fig. S13) illustrate well the nature of element-specific diagenetic

452 overprint of the four teeth. In samples with overall low [U] (<0.2 µg/g), i.e. Nadale 1 and

453 Fumane 2, there are no significant positive or negative correlations discernible. In case of

454 Riparo Broion 1 and Fumane 1, [U] rises up to 0.6 µg/g and positively correlates with Ba

455 and negatively with Mg, while Sr only shows significant co-variation in Riparo Broion 1.

456 It should be noted that spatially-resolved analysis by LA-ICPMS not only allows the

457 retrieval of time-resolved chemical signals, but is equally ideally-suited for the

458 delineation of well-preserved segments in partially diagenetically-overprinted samples.

459

460 Overall, we employ the following strategy to delineate well-preserved from

461 diagenetically overprinted segments in our enamel profiles. We stress that not a single

462 threshold value but rather a combination of the following criteria help delineate

463 diagenetically-overprinted from sufficiently well-preserved enamel domains:

464 1) The visible co-variation between U and Sr/Ca (Fig. 3) as well as above mentioned

465 correlations between Sr, Ba, Mg residuals with U (Fig. S13) show that especially Ba and

466 less so Sr (only Riparo Broion 1) were added during diagenesis, while Mg was lost.

467 Consequently, data segments with lowest U – below which no correlation remains ([U]

468 <~0.05 - 0.1 µg/g)- were used for further considerations. Incidentally, this 50 ppb [U]

469 threshold also matches well the enamel [U]-values for omnivores and carnivores from the

470 modern baseline study by (72).

471 2) The shape and nature of the discernible peaks/troughs provide an additional constraint.

472 Very sharp variations, over less than 5 days, in U, Ba, Mg in Fumane 1 (Fig. S10) and U,

473 Ba, Sr, Mg in Riparo Broion 1 (Fig. S11) characterize diagenetic signals, while variations

474 in low-U domains are far more gradual and occur over tens of days. The latter is more in

475 line with biologically-mediated variations that are additionally modulated by the

476 protracted nature of enamel mineralization (50), which precludes, for example, the up to

477 fourfold variability in Ba/Ca occurring at the profile start of Fumane 1 to be of in-vivo
478 origin (Fig. S10).

479 3) Diagenesis is highly sample-specific even at the same site, illustrated here for Fumane
480 cave, which makes a 'one size fits all' approach difficult to apply. While Fumane 2 is
481 almost not affected by diagenesis that does also not affect Ba or Mg, the only slightly
482 older Fumane 1 sample is more strongly overprinted, which manifests itself especially in
483 Ba addition (>twofold increase) and Mg loss, while Sr is little affected.

484

485 We note that diagenesis appears to affect the early formed enamel segments more than
486 later mineralized areas. As the former are characterized by higher enamel extension rates,
487 one conjecture is that this may have caused slightly greater amount of porosity that in
488 turn makes such domains more susceptible for post-mortem chemical overprint. Thus, the
489 initial portions of Nadale 1, Fumane 1 and Riparo Broion 1 crowns show enrichments in
490 U, Al and Mn, with a concurrent decrease of Mg (Figure 3 and S9-S12). While Sr seems
491 only partly affected by this overprint, Ba tends to precisely resemble the small-scale
492 chemical fluctuations of the diagenetic proxies (clearly visible in Riparo Broion 1 and
493 Fumane 1), suggesting a lack of post-burial stability for the latter element.

494 Taken together, we observe that the areas of interest (i.e. weaning onset) of our
495 specimens are sufficiently free from diagenetic alterations to reliably deduce time-
496 resolved dietary and mobility signals based on Sr/Ca and Sr isotopic ratios, respectively.

497

498
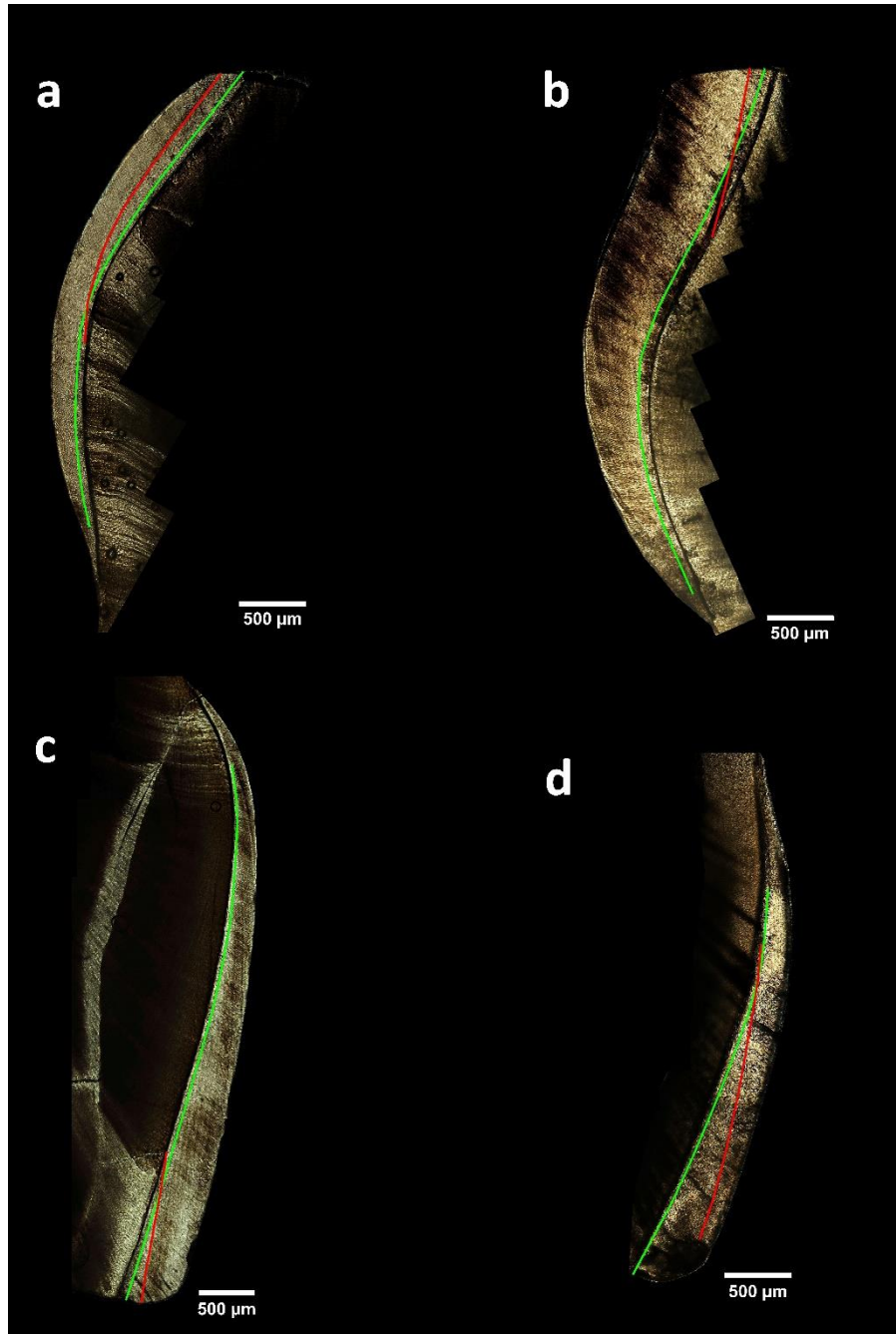
Figure S1. Micrographs acquired at 100x magnification of the four exfoliated deciduous fossil teeth. (a) Nadale 1, Neanderthal, lower right deciduous first molar, lingual aspect, the section pass through the metaconid; (b) Fumane 1, Neanderthal, lower left deciduous second molar, buccal aspect, he section pass through the hypoconid; (c) Riparo Broion 1, Neanderthal, upper left deciduous canine, buccal aspect; (d) Fumane 2, UPMH, upper right lateral deciduous incisor, buccal aspect. Red lines highlight the position of the Neonatal line marking birth event; green lines highlight the laser ablation paths.

a

B   L

O

M   ——   D

b

B   L

O

M   ——   D

c

B   L

O

M   ——   D

d

B   L

O

M   ——   D

507
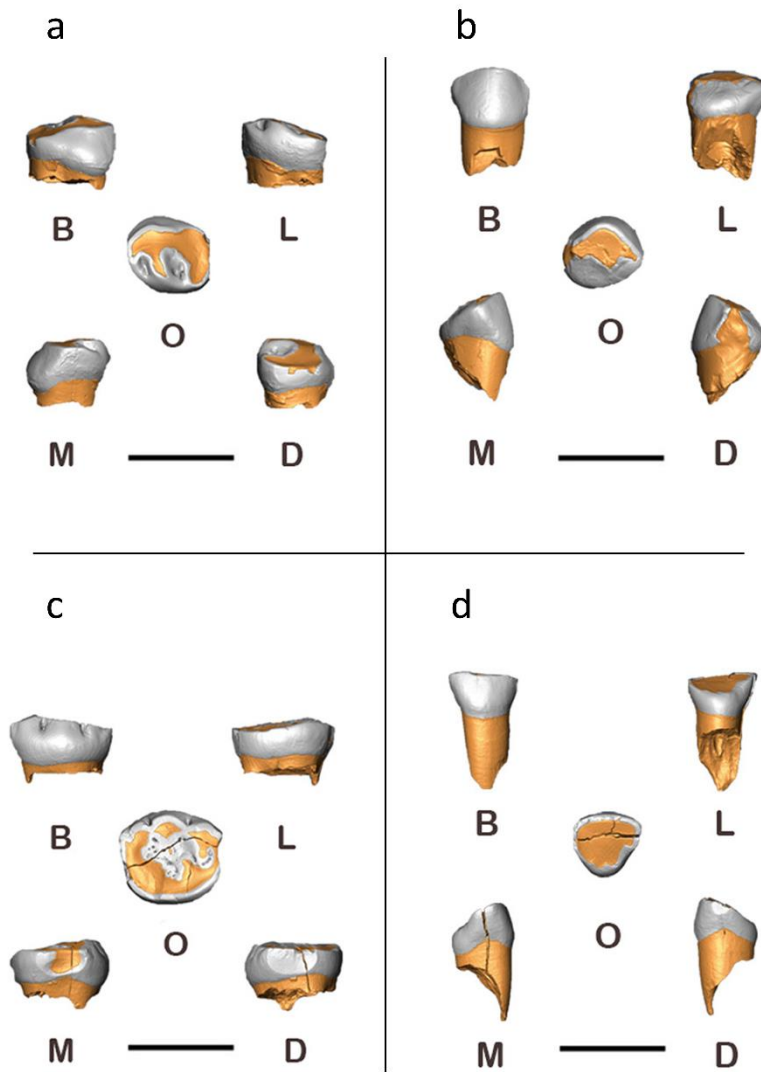
Figure S2. Three-dimensional digital models of the four exfoliated deciduous fossil teeth. (a) Nadale 1 (lower right first deciduous molar); (b) Fumane 1 (lower left second deciduous molar); (c) Riparo Broion 1 (upper right deciduous canine); (d) Fumane 2 (upper right lateral deciduous incisor). Scale bar 10 mm. B, buccal; D, distal; L, lingual; M, mesial; O, occlusal
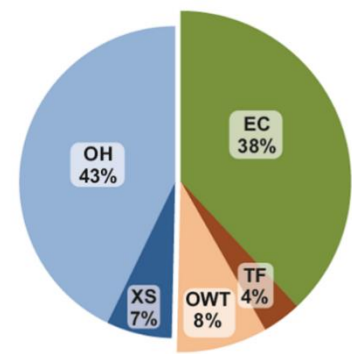
513
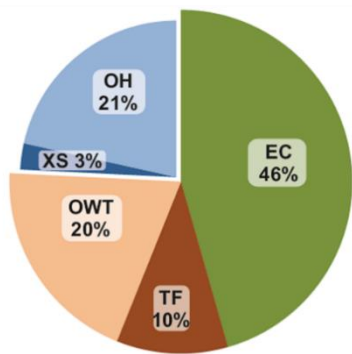
Fimon pollen record ca. 75-70 ka
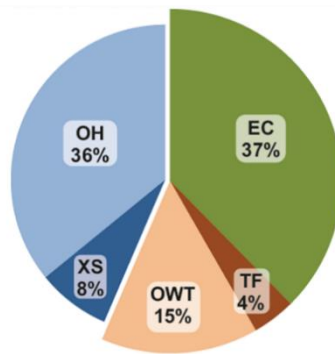
Fimon pollen record ca. 50-45 ka

Fimon pollen record ca. 45-40 ka

514

Figure S3. Pollen record summary of different vegetation types during selected time-frames. Pollen % are calculated based on the sum of terrestrial taxa and represent mean values over the selected time frame. Taxa are grouped according to their ecology and climatic preferences. Eurythermic conifers (EC): sum of *Pinus* and *Juniperus*; Temperate forest (TF): sum of deciduous *Quercus*, *Alnus glutinosa* type, *Fagus*, *Acer*, *Corylus, Carpinus, Fraxinus, Ulmus, Tilia* and *Salix*; Xerophytic steppe (XS): sum of *Artemisia* and Chenopodiaceae; other herbs (OH): sum of terrestrial herbs; other woody taxa (OWT) are also reported.

523
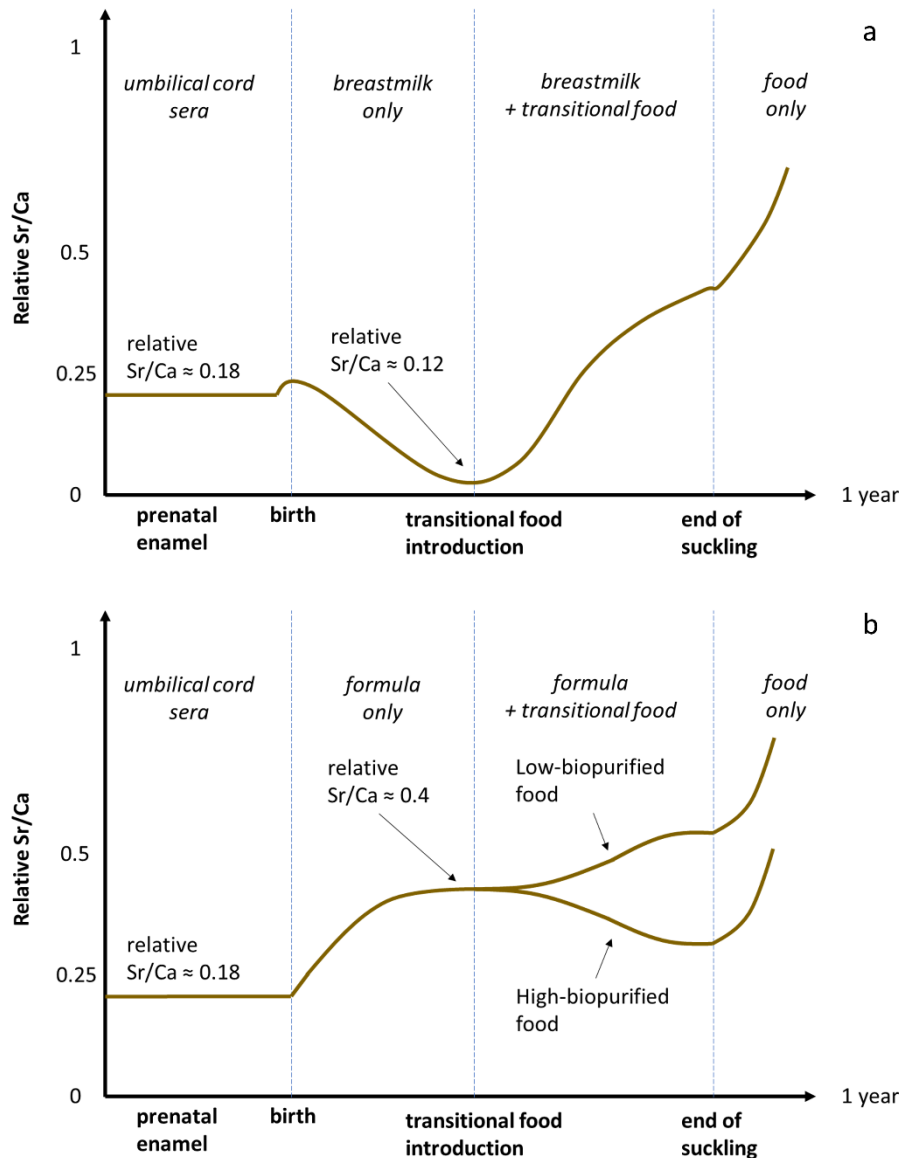
524
525 **Figure S4. Sr/Ca models for (a) breast-fed infants and (b) formula fed-infants.** These
526 models assume a mother diet equal to 1. In this model, GIT function is ignored since it
527 begins to significantly discriminate Sr over Ca at ~1 year of age in humans. A small peak
528 in Sr/Ca signal is visible across birth in breast-fed infants (a); this has been observed
529 empirically in our tooth samples and may relate to several factors, as e.g. high-metal
530 content of colostrum (57) or potential changes in perinatal physiology (56). The same
531 peak is probably masked in formula-fed infants (b) due to the rapid Sr/Ca increase.

532
533
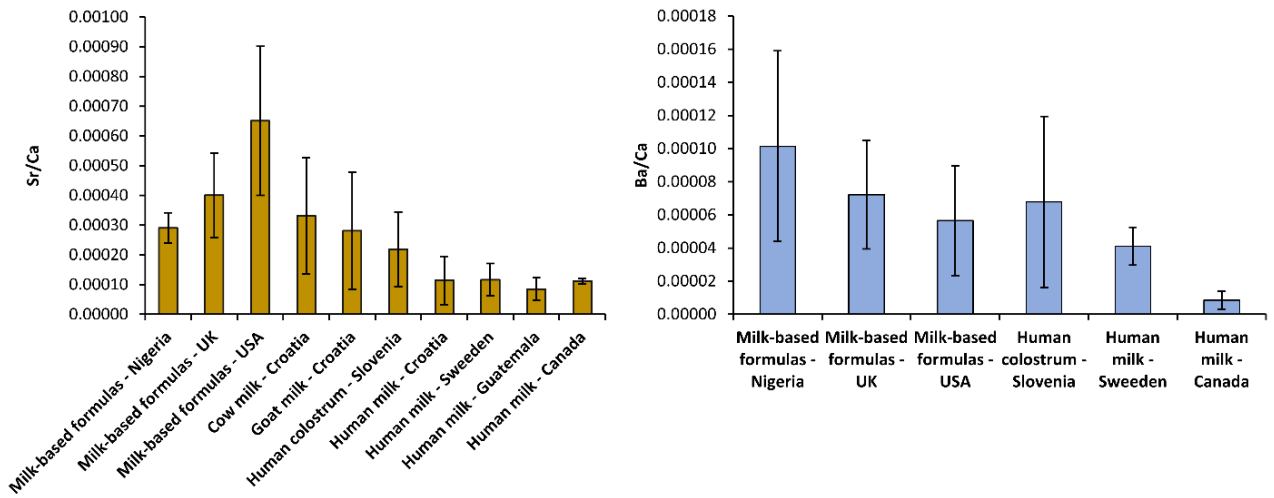
534
535
536 **Figure S5. Sr/Ca and Ba/Ca data of animal milks, human milks and formulas from**
537 **literature.** Formulas are from Ikem et al. (73); cow and goat milks are from Bilandžić et
538 al. (74); human colostrum is from Krachler et al. (55); human milks are from Bilandžić et
539 al. (74), Björklund et al. (75), Li et al. (76) and Friel et al. (77). The geographical
540 provenance of the samples is also reported. Error bars are standard deviations.
541

542

543
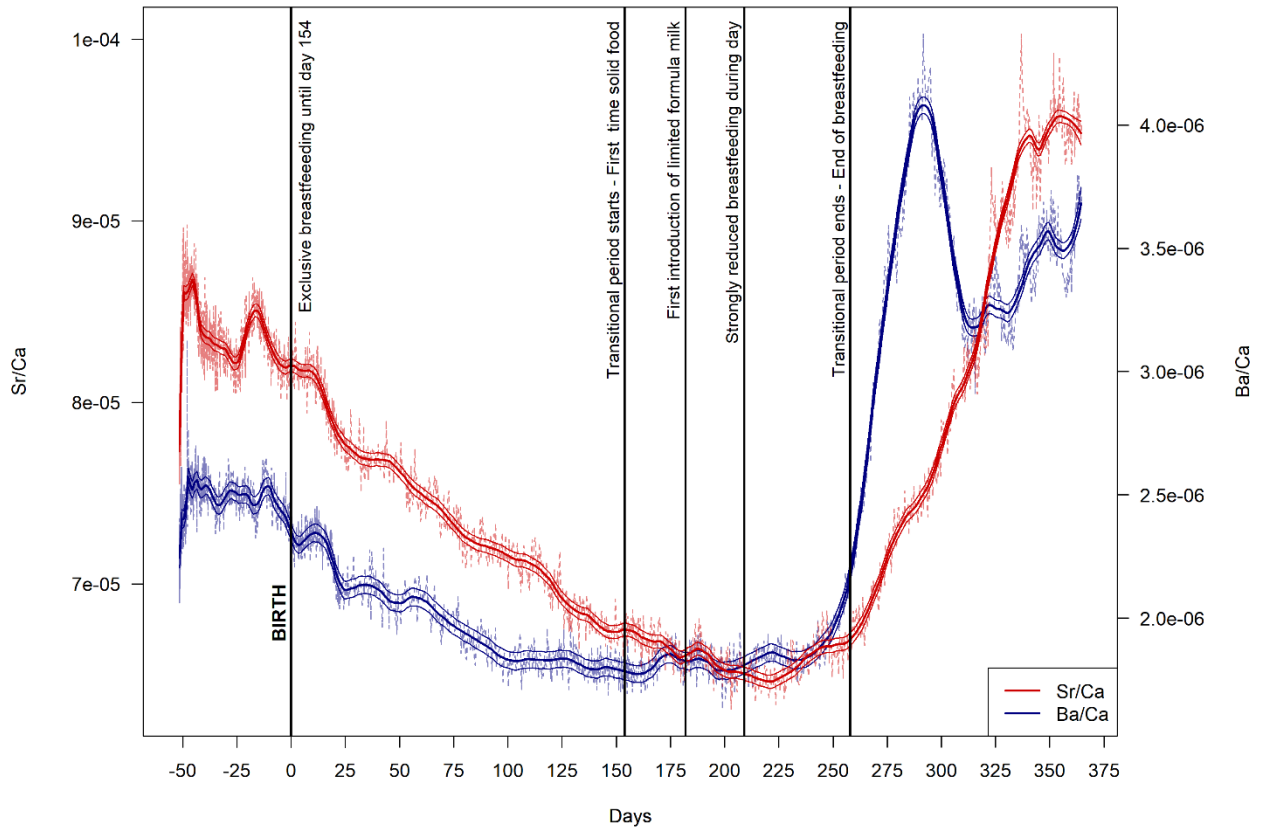
Figure S6. Time-resolved Sr/Ca and Ba/Ca profiles in modern reference deciduous teeth of the exclusively breastfed individual MCS1. Deciduous second molar dm2; The elemental profiles were analyzed within enamel closest to the enamel-dentine-junction (EDJ).

548

549
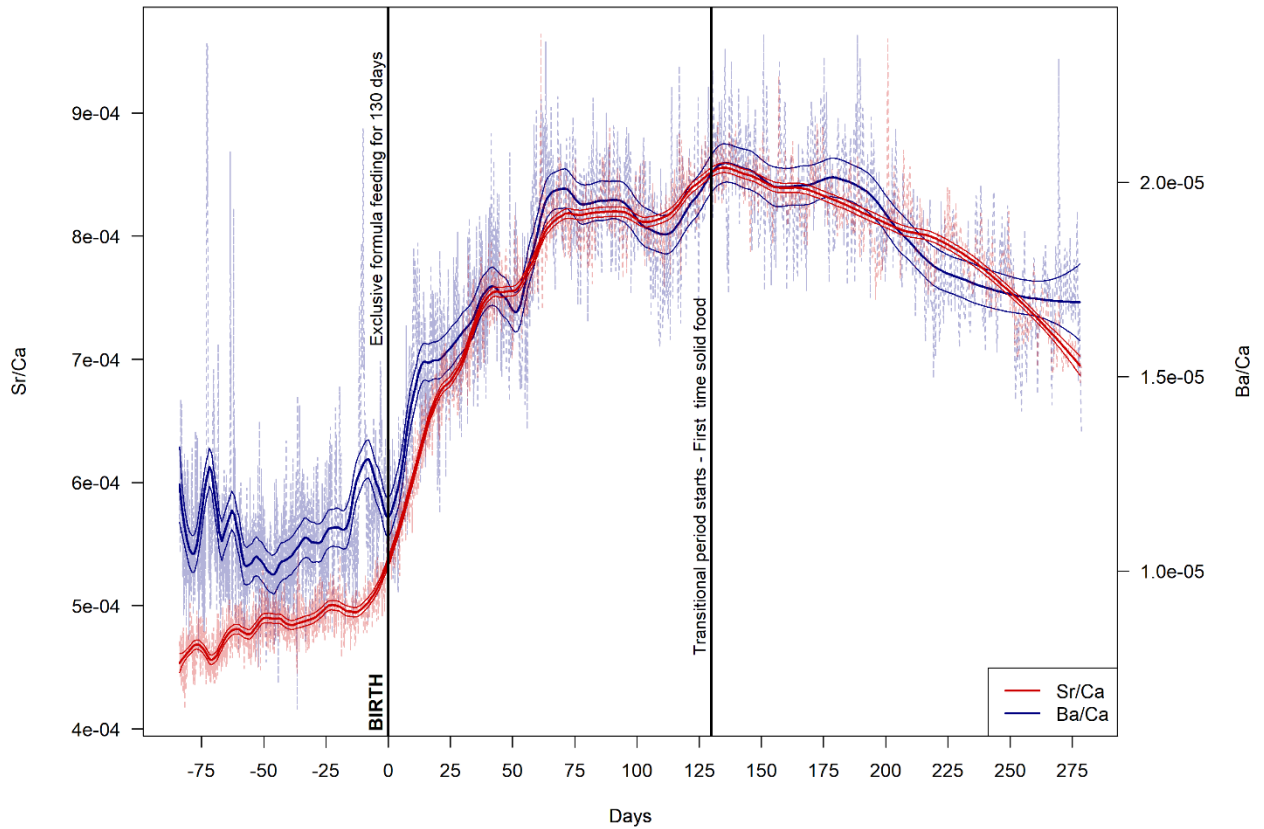
Figure S7. Time-resolved Sr/Ca and Ba/Ca profiles in modern reference deciduous teeth of the exclusively formula-fed individual MCS2. Deciduous canine dc. The elemental profiles were analyzed within enamel closest to the enamel-dentine-junction (EDJ).

554

555

Figure S8. Time-resolved Sr/Ca and Ba/Ca profiles in modern reference deciduous teeth of the mixed breast- formula-fed individual **individual MCS3.** deciduous canine dc. The elemental profiles were analyzed within enamel closest to the enamel-dentine-junction (EDJ).

560
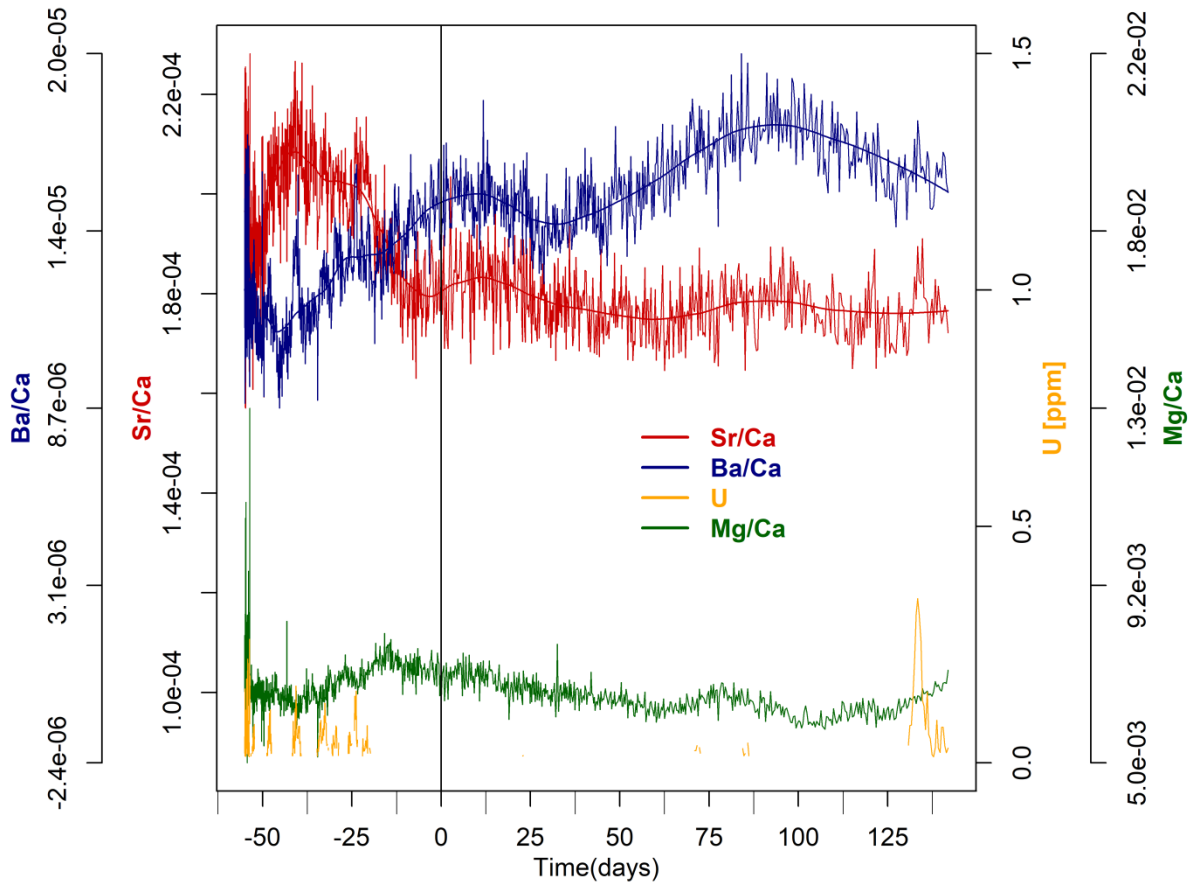
561
562
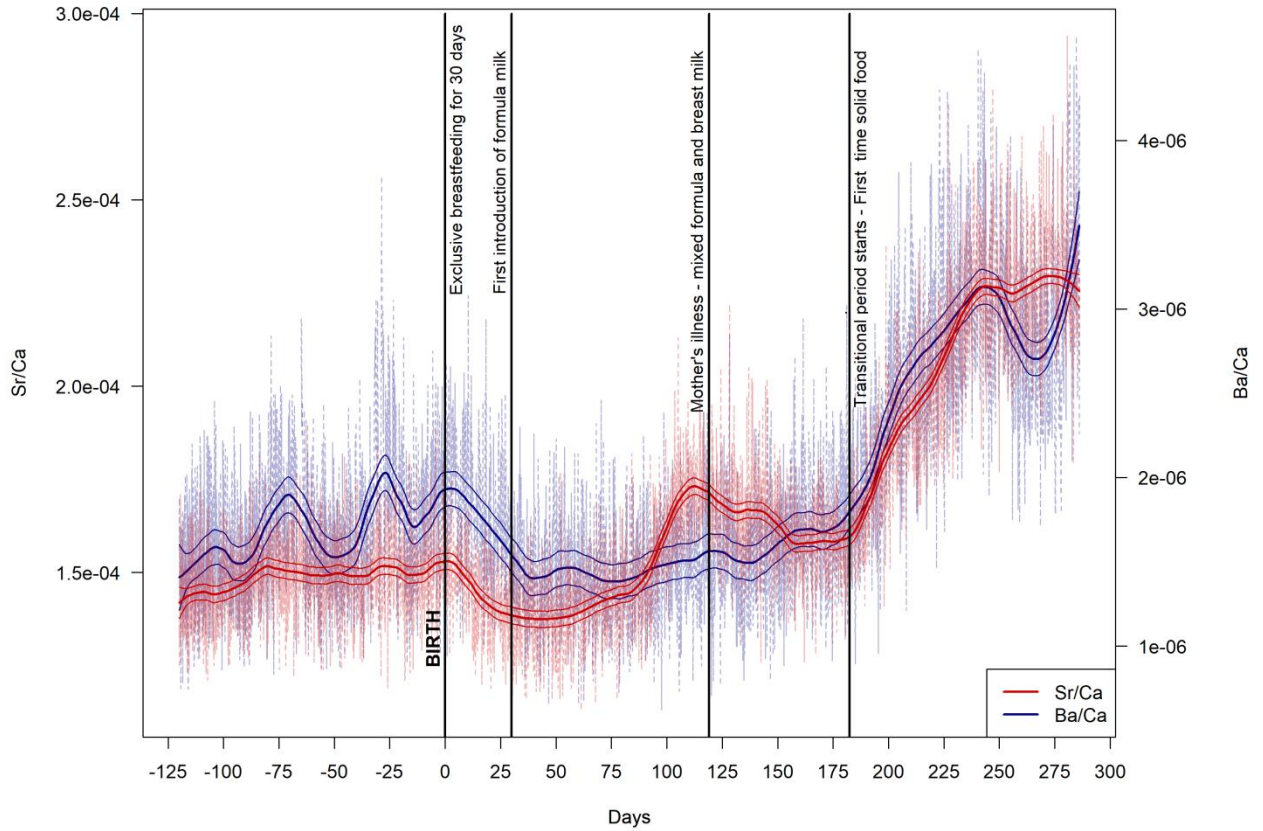**Figure S9. Time-resolved Sr/Ca, Ba/Ca, Mg/Ca and [U] profiles Nadale 1 deciduous**
563
teeth. The elemental profiles were analyzed within enamel closest to the enamel-dentine-
564
junction (EDJ).
565

566

567

Figure S10. Time-resolved Sr/Ca, Ba/Ca, Mg/Ca and [U] profiles Fumane 1 deciduous teeth. The elemental profiles were analyzed within enamel closest to the enamel-dentine-junction (EDJ); While Sr seems only partly affected by this overprint, Ba tends to precisely resemble the small-scale chemical fluctuations of the diagenetic proxies (i.e. U). The anticorrelation between U and Mg/Ca indicates a loss Mg during the post-burial history, and the likely precipitation of low-Mg phases. Black arrows highlight the worst diagenetically-affected domains of the enamel.

575

576

Figure S11. Time-resolved Sr/Ca, Ba/Ca, Mg/Ca and [U] profiles Riparo Broion 1 deciduous teeth. The elemental profiles were analyzed within enamel closest to the enamel-dentine-junction (EDJ); While Sr seems only partly affected by this overprint, Ba tends to precisely resemble the small-scale chemical fluctuations of the diagenetic proxies (i.e. U). The anticorrelation between U and Mg/Ca indicates a loss Mg during the post-burial history, and the likely precipitation of low-Mg phases. Black arrows highlight the worst diagenetically-affected domains of the enamel.
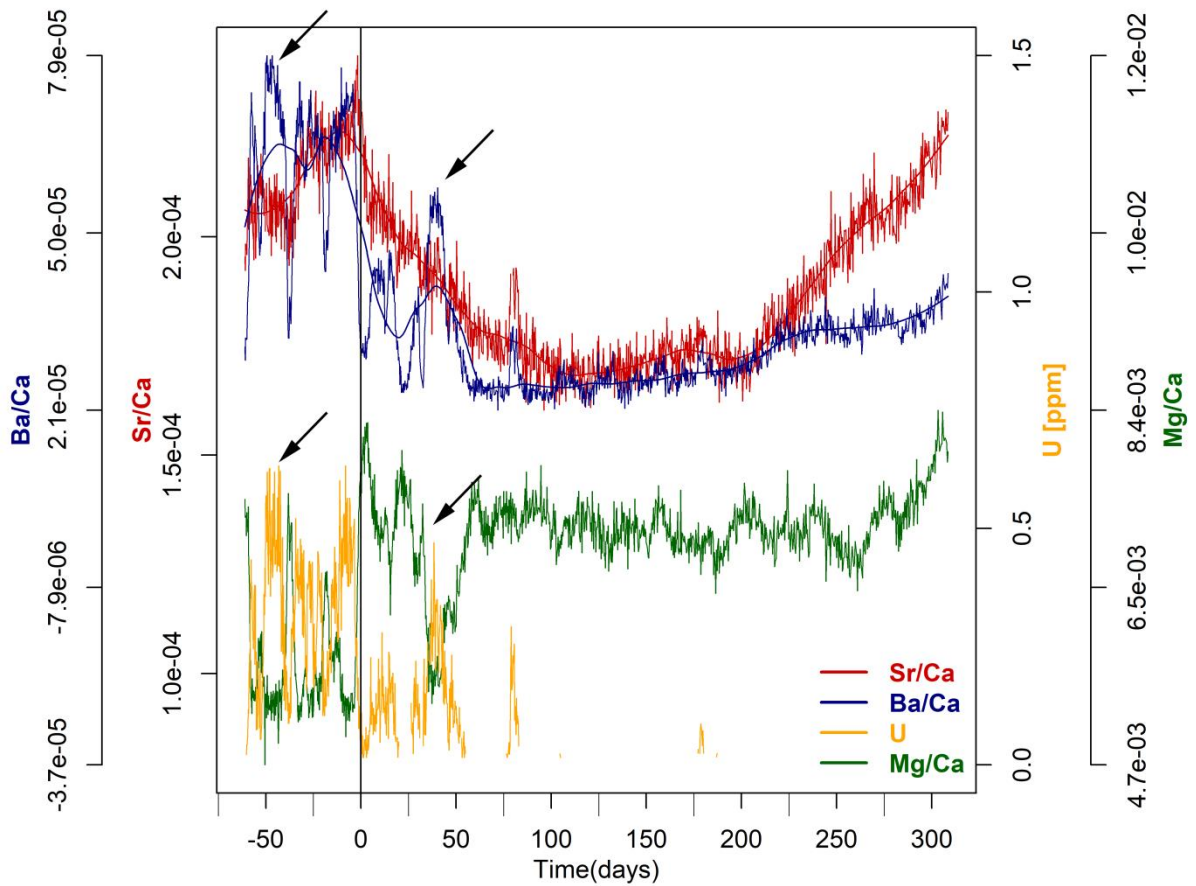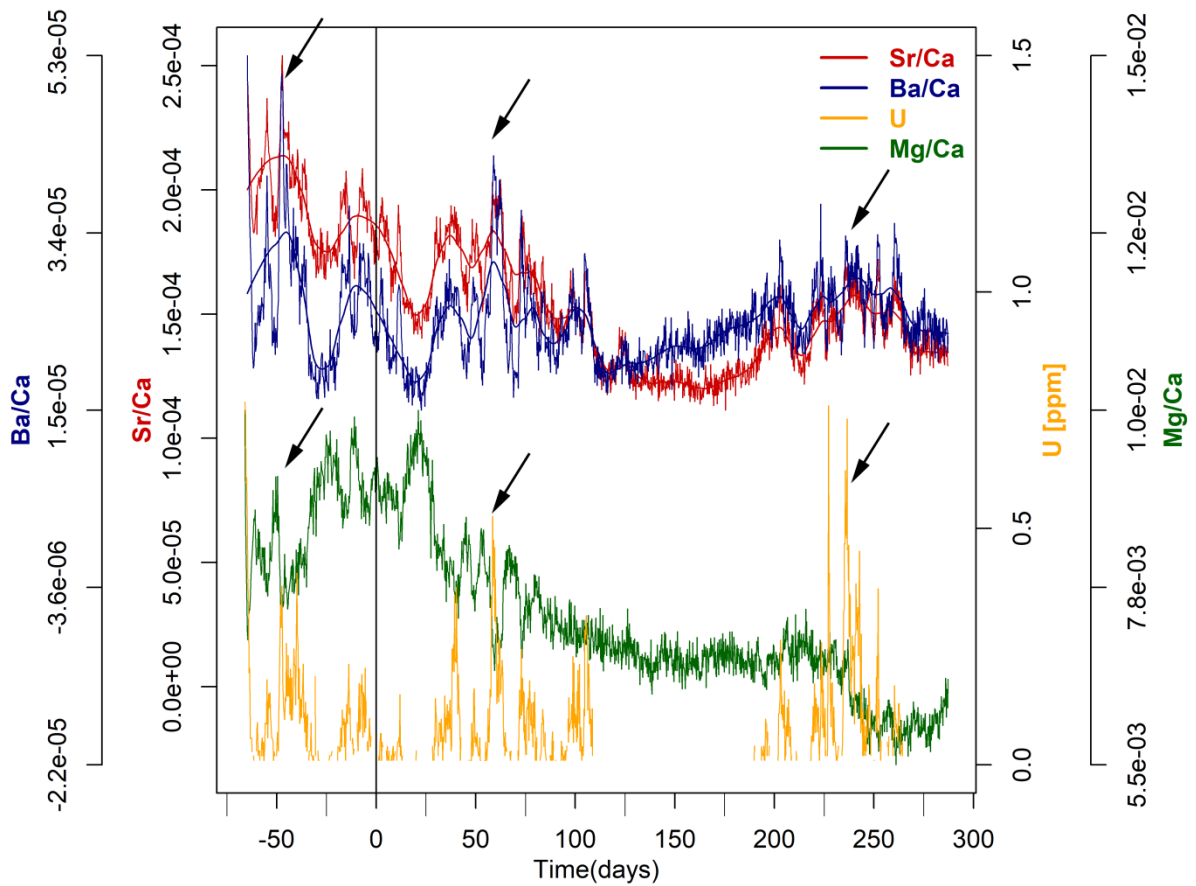
584

585
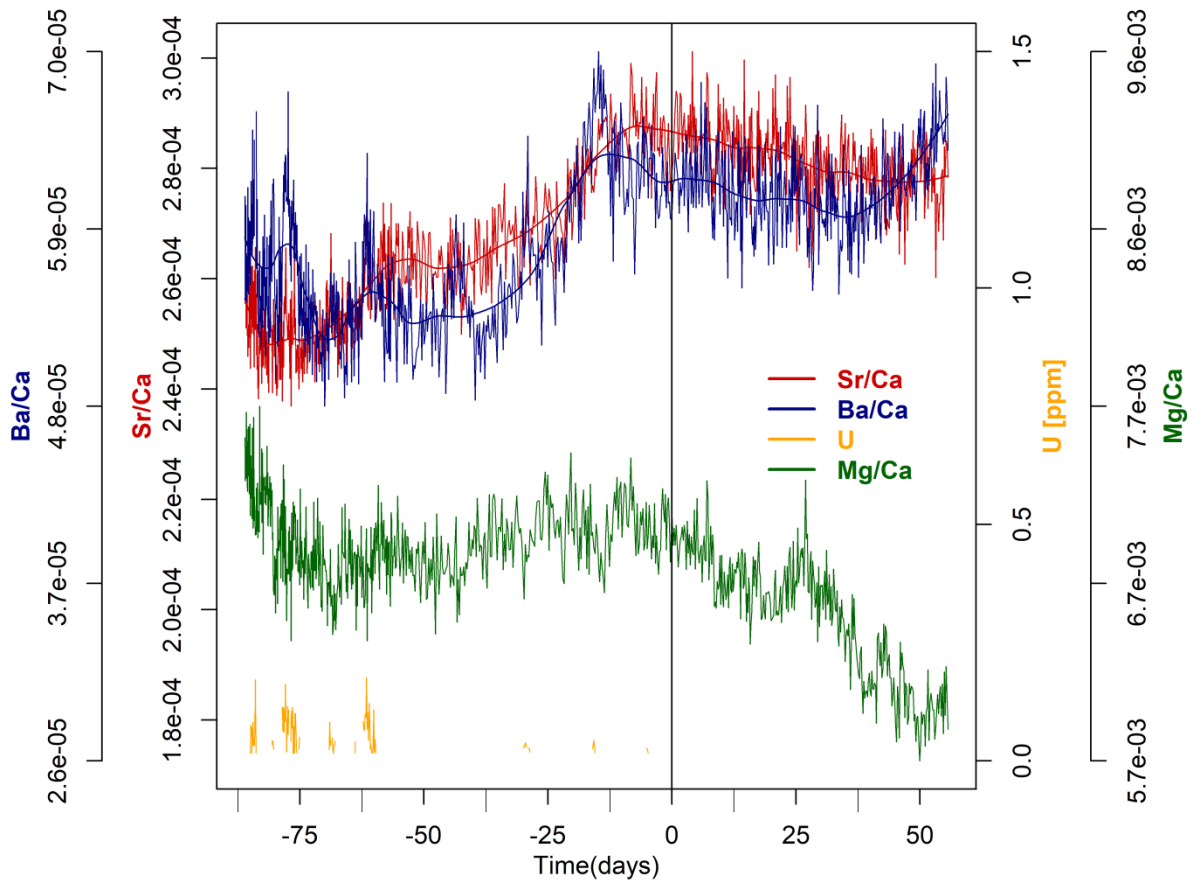
Figure S12. Time-resolved Sr/Ca, Ba/Ca, Mg/Ca and [U] profiles Fumane 2
586
deciduous tooth. The elemental profiles were analyzed within enamel closest to the
587
enamel-dentine-junction (EDJ).
588

589
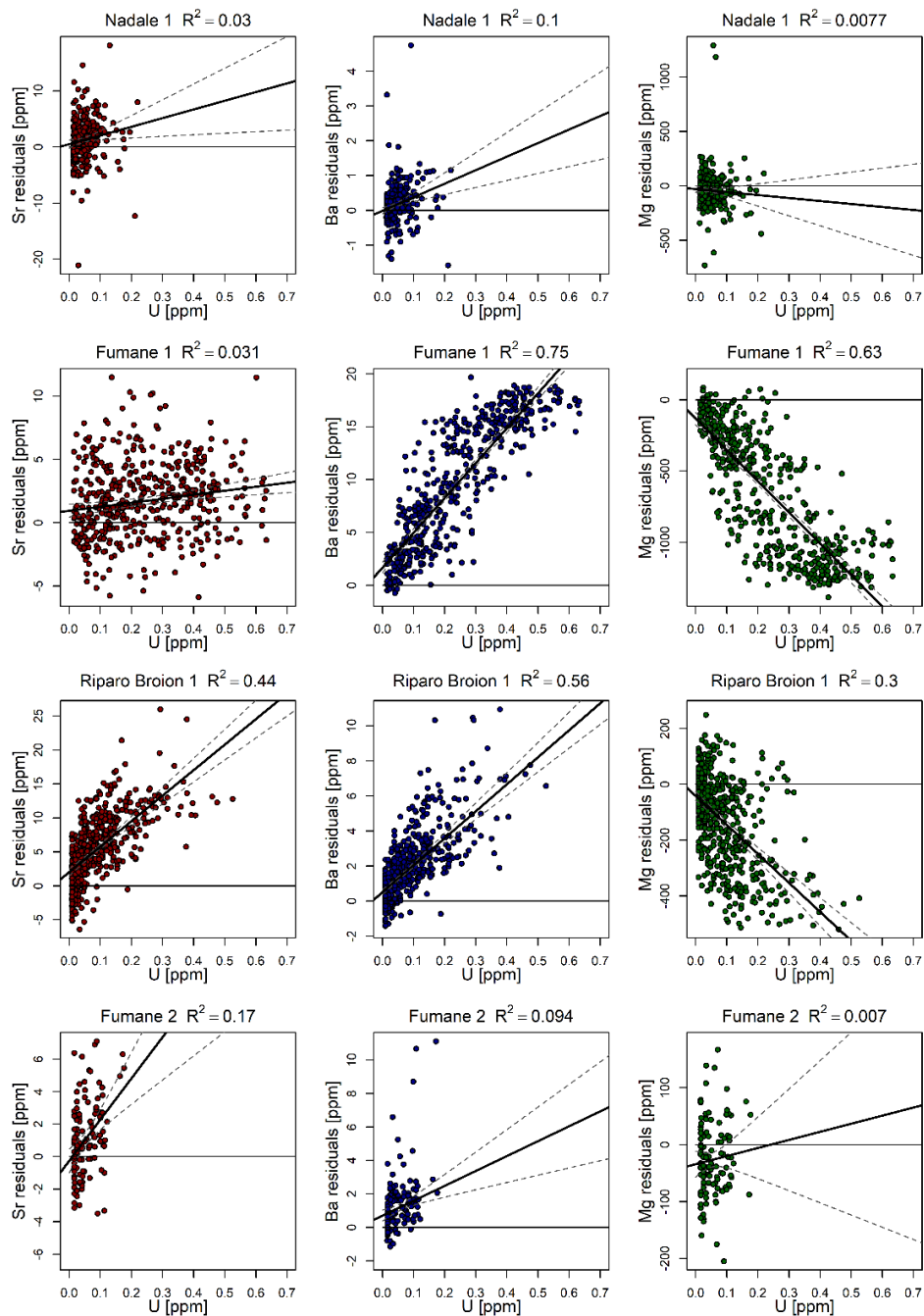
Fig. S13: Scatter plots of U vs. the residuals of Sr, Ba or Mg variation for the diagenetically most affected segments in Nadale 1 (start till -10days), Fumane 1 (start till 100 days), Riparo Broion 1(start till 125 days) and Fumane 2 (start till -50 days). Residuals were derived from the smoothed elemental profiles of Fig. 3e, calculated with a local polynomial regression fitting - LOWESS (78) - on the laser path portions with U≤LOD. The residual Sr, Ba, Mg variability rather all data were used as we wanted as much as possible remove biological variation overprint any diagenesis signal.

Table S1: Sr isotopes of local rodent teeth by MC-ICPMS

Site	Local geology	Rodent species	Sample type	$^{87}Sr/^{87}Sr$	2 S.E.
Nadale	Eocene limestone	*Microtinae* indet.	enamel	0.70847	0.00001
			enamel	0.70843	0.00001
			enamel	0.70825	0.00003
			enamel	0.70864	0.00001
			enamel	0.70857	0.00001
			mean (± 2 S.D.)	**0.70847**	**0.00030**
Riparo Broion	Eocene Oligocene limestone	*Microtinae* indet.	whole tooth	0.70826	0.00001
			whole tooth	0.70820	0.00001
			whole tooth	0.70814	0.00001
			whole tooth	0.70827	0.00001
			whole tooth	0.70838	0.00001
			mean (± 2 S.D.)	**0.70825**	**0.00018**
Fumane Cave	Jurassic-Cretaceous limestone and marl	*Microtinae* indet.	enamel	0.70948	0.00001
			enamel	0.70937	0.00001
			enamel	0.70947	0.00001
			enamel	0.70940	0.00001
			enamel	0.70962	0.00001
			enamel	0.70958	0.00001
			mean (± 2 S.D.)	**0.70948**	**0.00020**

598

599

600 **Table S2.** Discrimination factors of Sr over Ca within mother and infant bodies; fluxes
601 through different tissues are reported in brackets; a Sr/Ca relative to a mother diet equal
602 to 1 has been calculated for each end-member; the different enamel portions where a
603 specific signal is fixed are also reported.

End-member (flux)	(Sr-over-Ca discrimination factor)	Relative Sr/Ca	Reference	Enamel
Diet	-	**1**	-	-
Mother sera (diet-blood)	0.30 ± 0.08*	**0.3**	Balter, 2004	-
Umbilical cord sera (mother sera - placenta)	0.6	**0.18**	ICRP, 2004	prenatal
Breastmilk (mother sera - mammary gland)	0.4	**0.12**	ICRP, 2004	postnatal, breast-fed infant
Animal milk	One trophic level lower than human breastmilk (Sr/Ca ~3.3-fold higher than human milk)	**0.40**	Balter, 2004; see text	postnatal, formula-fed infant

*this value is relative to the difference between mammals' muscle (or bone) tissue and their diet, based on a large trophic chain study; for simplicity any eventual discrimination between blood and muscles (or bones) is ignored.

604

605

606 **Table S3**. Ba, Sr, Ca, Ba/Ca and Sr/Ca values of umbilical cord sera, breast-fed infant
607 sera and formula-fed infant sera from (52, 55). Values are reported as mean ± sd.

Elemental contents and ratios	Maternal sera[a]	Umbilical cord sera[b]	Umbilical cord sera[a]	Breast-fed infant (ca. 3 months) sera[b]	Formula-fed infant (ca. 3 months) sera[b]	Colostrum[a]
Ba (µg/L)	6 ± 7.8	0.8 ± 0.8	1.5 ± 1.7	1.9 ± 0.4	3.8 ± 1.4	10.6 ± 8.7
Sr (µg/L)	22.3 ± 8.9	20 ± 9	19.6 ± 7.2	12 ± 3	40 ± 25	37 ± 18
Ca (mg/L)	92 ± 16	95 ± 13	104 ± 16	112 ± 4	116 ± 8	210 ± 60
Ba/Ca*10³	0.082 ± 0.099	0.010 ± 0.010	0.017 ± 0.019	0.017 ± 0.004	0.034 ± 0.014	0.068 ± 0.061
Sr/Ca*10³	0.267 ± 0.143	0.228 ± 0.126	0.204 ± 0.101	0.108 ± 0.031	0.361 ± 0.240	0.219 ± 0.148

[a]Krachler et al. (1999, *European Journal of Clinical Nutrition*); [b]Krachler et al. (1999, *Biological Trace Element Research*).

608

609

Legends for Datasets

611

612 **Dataset S1**. $^{87}Sr/^{86}Sr$, $^{84}Sr/^{86}Sr$ and $^{85}Rb/^{86}Sr$ data of Middle-Upper Paleolithic deciduous
613 teeth (baseline, interference, mass-bias/elemental-fractionation-corrected (see text); very
614 minor offset of $^{84}Sr/^{86}Sr$ from 0.0565 is due to residual variability of ^{84}Kr-backgrounds
615 for protracted profile analyses).

616

617 **Dataset S2**. Sr/Ca and Ba/Ca data of modern reference deciduous teeth.

618

619 **Dataset S3**. Sr/Ca, Ba/Ca, Mg/Ca and [U] data of Middle-Upper Paleolithic deciduous
620 teeth (LOD indicates that [U]<limit of detection).

621

622 **SI References**

623

624 1. Benazzi S, *et al.* (2014) Middle Paleolithic and Uluzzian human remains from
625 Fumane Cave, Italy. *Journal of Human Evolution* 70:61-68.
626 2. Arnaud J, *et al.* (2017) A Neanderthal deciduous human molar with incipient
627 carious infection from the Middle Palaeolithic De Nadale cave, Italy. *American*
628 *Journal of Physical Anthropology* 162(2):370-376.
629 3. Benazzi S, *et al.* (2015) The makers of the Protoaurignacian and implications for
630 Neandertal extinction. *Science* 348(6236):793-796.
631 4. AlQahtani SJ, Hector M, & Liversidge H (2010) Brief communication: the
632 London atlas of human tooth development and eruption. *American Journal of*
633 *Physical Anthropology* 142(3):481-490.
634 5. Jequier CA, *et al.* (2015) The De Nadale Cave, a single layered Quina Mousterian
635 site in the North of Italy. *Quartär* 62 (2015): 7-21.
636 6. Livraghi A, Fanfarillo G, Dal Colle M, Romandini M, & Peresani M (2019)
637 Neanderthal ecology and the exploitation of cervids and bovids at the onset of
638 MIS4: A study on De Nadale cave, Italy. *Quaternary International*.
639 7. Terlato G, Livraghi A, Romandini M, & Peresani M (2019) Large bovids on the
640 Neanderthal menu: Exploitation of Bison priscus and Bos primigenius in
641 northeastern Italy. *Journal of Archaeological Science: Reports* 25:129-143.
642 8. López-García JM, Livraghi A, Romandini M, & Peresani M (2018) The De
643 Nadale Cave (Zovencedo, Berici Hills, northeastern Italy): A small-mammal
644 fauna from near the onset of Marine Isotope Stage 4 and its palaeoclimatic
645 implications. *Palaeogeography, Palaeoclimatology, Palaeoecology* 506:196-201.
646 9. Martellotta E, Livraghi A, & Peresani M (in press) Bone retouchers from the
647 Mousterian Quina site of De Nadale Cave (Berici Hills, north-eastern Italy).
648 *Comptes Rendu Palevol*.
649 10. Broglio A, Cilli C, Giacobini G, & Gurioli F (2006) Osso, palco, dente e
650 conchiglia: i supporti in materia dura animale dei manufatti dei primi uomini
651 moderni a Fumane (Verona). *XXXIX Riunione Scientifica Istituto Italiano*
652 *Preistoria e Protostoria" Materie prime e scambi nella preistoria italiana"*,
653 (Istituto Italiano Preistoria e Protostoria), pp 815-827.
654 11. Peresani M (2012) Fifty thousand years of flint knapping and tool shaping across
655 the Mousterian and Uluzzian sequence of Fumane cave. *Quaternary International*
656 247:125-150.
657 12. Peresani M, Cristiani E, & Romandini M (2016) The Uluzzian technology of
658 Grotta di Fumane and its implication for reconstructing cultural dynamics in the
659 Middle–Upper Palaeolithic transition of Western Eurasia. *Journal of Human*
660 *Evolution* 91:36-56.
661 13. Peresani M, *et al.* (2008) Age of the final Middle Palaeolithic and Uluzzian levels
662 at Fumane Cave, Northern Italy, using 14C, ESR, 234U/230Th and
663 thermoluminescence methods. *Journal of Archaeological Science* 35(11):2986-
664 2996.

665   14.   Higham T, *et al.* (2009) Problems with radiocarbon dating the Middle to Upper
666   Palaeolithic transition in Italy. *Quaternary Science Reviews* 28(13-14):1257-1267.
667   15.   López-García JM, dalla Valle C, Cremaschi M, & Peresani M (2015)
668   Reconstruction of the Neanderthal and Modern Human landscape and climate
669   from the Fumane cave sequence (Verona, Italy) using small-mammal
670   assemblages. *Quaternary Science Reviews* 128:1-13.
671   16.   Fiore I, Gala M, & Tagliacozzo A (2004) Ecology and subsistence strategies in
672   the Eastern Italian Alps during the Middle Palaeolithic. *International Journal of*
673   *Osteoarchaeology* 14(3-4):273-286.
674   17.   Falcucci A, Conard NJ, & Peresani M (2017) A critical assessment of the
675   Protoaurignacian lithic technology at Fumane Cave and its implications for the
676   definition of the earliest Aurignacian. *PloS one* 12(12).
677   18.   Falcucci A, Peresani M, Roussel M, Normand C, & Soressi M (2018) What's the
678   point? Retouched bladelet variability in the Protoaurignacian. Results from
679   Fumane, Isturitz, and Les Cottés. *Archaeological and Anthropological Sciences*
680   10(3):539-554.
681   19.   Peresani M, *et al.* (2019) Marine and freshwater shell exploitation in the Early
682   Upper Palaeolithic. Re-examination of the assemblages from Fumane Cave (NE
683   Italy). *PaleoAnthropology* 2019, 64–81
684   20.   Cavallo G, *et al.* (2018) Heat Treatment of Mineral Pigment During the Upper
685   Palaeolithic in North-East Italy. *Archaeometry* 60(5):1045-1061.
686   21.   Peretto C, Biagi P, Boschian G, & Broglio A (2004) Living-floors and structures
687   from the Lower Paleolithic to the Bronze Age in Italy. *Collegium Antropologicum*
688   28(1):63-88.
689   22.   Broglio A, *et al.* (2003) L'Aurignacien dans le territoire préalpin: la Grotte de
690   Fumane. *XIV UISPP Congress*, (British Archaeological Reports), pp 93-104.
691   23.   Cassoli P & Tagliacozzo A (1994) Considerazioni paleontologiche,
692   paleoecologiche e archeozoologiche sui macromammiferi e gli uccelli dei livelli
693   del Pleistocene superiore del Riparo di Fumane (VR) scavi 1988–91. *Bollettino*
694   *del Museo civico di Storia Naturale di Verona* 18:349-445.
695   24.   Broglio A, Bertola S, De Stefani M, & Gurioli F (2009) "The shouldered points of
696   the Early Epigravettian of the Berici Hills (Venetian Region–North Italy).
697   Materials, Blanks, Typology, Exploitation" in Understanding the Past. Papers
698   offered to Stefan K. Kozlowski. Center for Research on the Antiquity of
699   Southeastern Europe. University of Warsaw, Warsaw: 59-68.
700   25.   Sauro U (2002) The Monti Berici: a peculiar type of karst in the Southern Alps.
701   *Acta Carsologica* 31(3):99-114.
702   26.   Dal Lago A & Mietto P (2003) Grotte dei Berici. *Aspetti fisici e naturalistici.*
703   Museo Naturalistico Archeologico, Vicenza.
704   27.   Peresani M & Porraz G (2004) Ré-interprétation et mise en valeur des niveaux
705   moustériens de la Grotte du Broion (Monti Berici, Vénétie). Etude techno-
706   économique des industries lithiques.
707   28.   Romandini M, Bertola S, & Nannini N (2015) Nuovi dati sul Paleolitico dei Colli
708   Berici: risultati preliminari dello studio archeozoologico e delle materie prime
709   litiche della Grotta del Buso Doppio del Broion (Lumignano, Longare, Vicenza).

710   *Nuovi dati sul Paleolitico dei Colli Berici: risultati preliminari dello studio*
711   *archeozoologico e delle materie prime litiche della Grotta del Buso Doppio del*
712   *Broion (Lumignano, Longare, Vicenza)*:53-59.

713   29.   De Stefani M, Gurioli F, & Ziggiotti S (2005) Il Paleolitico superiore del Riparo
714   del Broion nei Colli Berici (Vicenza). *Il Paleolitico superiore del Riparo del*
715   *Broion nei Colli Berici (Vicenza)*:93-108.

716   30.   Peresani M, Bertola S, Delpiano D, Benazzi S, & Romandini M (2019) The
717   Uluzzian in the north of Italy: insights around the new evidence at Riparo Broion.
718   *Archaeological and Anthropological Sciences* 11(7):3503-3536.

719   31.   Romandini M, *et al.* (2020) A late Neanderthal tooth from northeastern Italy.
720   *Journal of Human Evolution* **147**, 102867.

721   32.   Vescovi E, *et al.* (2007) Interactions between climate and vegetation on the
722   southern side of the Alps and adjacent areas during the Late-glacial period as
723   recorded by lake and mire sediment archives. *Quaternary Science Reviews*
724   26:1650-1669.

725   33.   Badino F, *et al.* (2019) An overview of Alpine and Mediterranean
726   palaeogeography, terrestrial ecosystems and climate history during MIS 3 with
727   focus on the Middle to Upper Palaeolithic transition. *Quaternary International*.

728   34.   Pini R, Ravazzi C, & Reimer P (2010) The vegetation and climate history of the
729   last glacial cycle in a new pollen record from Lake Fimon (southern Alpine
730   foreland, N-Italy). *Quaternary Science Reviews* 29(23-24):3115-3137.

731   35.   Shannon R (1976) Revised effective ionic radii and systematic studies of
732   interatomic distances in halides and chalcogenides. *Acta crystallographica section*
733   *A: crystal physics, diffraction, theoretical and general crystallography* 32(5):751-
734   767.

735   36.   Burton JH, Price TD, & Middleton WD (1999) Correlation of bone Ba/Ca and
736   Sr/Ca due to biological purification of calcium. *Journal of Archaeological*
737   *Sciences* 26(6):609-616.

738   37.   Elias RW, Hirao Y, & Patterson CC (1982) The Circumvention of the Natural
739   Biopurification of Calcium along Nutrient Pathways by Atmospheric Inputs of
740   Industrial Lead. *Geochimica et Cosmochimica Acta* 46(12):2561-2580.

741   38.   Balter V (2004) Allometric constraints on Sr/Ca and Ba/Ca partitioning in
742   terrestrial mammalian trophic chains. *Oecologia* 139(1):83-88.

743   39.   Dahl S, *et al.* (2001) Incorporation and distribution of strontium in bone. *Bone*
744   28(4):446-453.

745   40.   Kshirsagar S, Lloyd E, & Vaughan J (1966) Discrimination between strontium
746   and calcium in bone and the transfer from blood to bone in the rabbit. *The British*
747   *Journal of Radiology* 39(458):131-140.

748   41.   Burton JH & Wright LE (1995) Nonlinearity in the relationship between bone
749   Sr/Ca and diet: paleodietary implications. *American Journal of Physical*
750   *Anthropology* 96(3):273-282.

751   42.   Price TD, Swick RW, & Chase EP (1986) Bone chemistry and prehistoric diet:
752   strontium studies of laboratory rats. *American Journal of Physical Anthropology*
753   70(3):365-375.

754 43. Gilbert C, Sealy J, & Sillen A (1994) An investigation of barium, calcium and
755   strontium as palaeodietary indicators in the Southwestern Cape, South Africa.
756   *Journal of Archaeological Science* 21(2):173-184.
757 44. Rivera J & Harley JH (1965) The HASL Bone Program, 1961-1964. (Health and
758   Safety Lab., New York Operations Office (AEC), NY).
759 45. Sillen A & Smith P (1984) Weaning patterns are reflected in strontium-calcium
760   ratios of juvenile skeletons. *Journal of Archaeological Science* 11(3):237-245.
761 46. Lough S, Rivera J, & Comar C (1963) Retention of strontium, calcium, and
762   phosphorus in human infants. *Proceedings of the Society for Experimental*
763   *Biology and Medicine* 112(3):631-636.
764 47. Rossipal E, Krachler M, Li F, & Micetic-Turk D (2000) Investigation of the
765   transport of trace elements across barriers in humans: studies of placental and
766   mammary transfer. *Acta Paediatrica* 89(10):1190-1195.
767 48. ICRP (2004) Doses to infants from ingestion of radionuclides in mother's milk.
768   *ICRP Publication 95. Ann. ICRP* 34(3–4).
769 49. Humphrey LT, Dean MC, Jeffries TE, & Penn M (2008) Unlocking evidence of
770   early diet from tooth enamel. *Proceedings of the National Academy of Sciences of*
771   *the United States of America* 105(19):6834-6839.
772 50. Müller W, *et al.* (2019) Enamel mineralization and compositional time-resolution
773   in human teeth evaluated via histologically-defined LA-ICPMS profiles.
774   *Geochimica et Cosmochimica Acta* 255:105-126.
775 51. Humphrey LT, Dirks W, Dean MC, & Jeffries TE (2008) Tracking dietary
776   transitions in weanling baboons (Papio hamadryas anubis) using
777   strontium/calcium ratios in enamel. *Folia Primatologica* 79(4):197-212.
778 52. Krachler M, Rossipal E, & Micetic-Turk D (1999) Concentrations of trace
779   elements in sera of newborns, young infants, and adults. *Biological trace element*
780   *research* 68(2):121.
781 53. Peek S & Clementz MT (2012) Sr/Ca and Ba/Ca variations in environmental and
782   biological sources: a survey of marine and terrestrial systems. *Geochimica et*
783   *Cosmochimica Acta* 95:36-52.
784 54. Austin C, *et al.* (2013) Barium distributions in teeth reveal early-life dietary
785   transitions in primates. *Nature* 498(7453):216-219.
786 55. Krachler M, Rossipal E, & Micetic-Turk D (1999) Trace element transfer from
787   the mother to the newborn—investigations on triplets of colostrum, maternal and
788   umbilical cord sera. *European Journal of Clinical Nutrition* 53(6):486-494.
789 56. Dean MC, Spiers KM, Garrevoet J, & Le Cabec A (2019) Synchrotron X-ray
790   fluorescence mapping of Ca, Sr and Zn at the neonatal line in human deciduous
791   teeth reflects changing perinatal physiology. *Archives of Oral Biology* 104:90-
792   102.
793 57. Matos C, Moutinho C, Almeida C, Guerra A, & Balcão V (2014) Trace element
794   compositional changes in human milk during the first four months of lactation.
795   *International Journal of Food Sciences and Nutrition* 65(5):547-551.
796 58. Metcalfe JZ, Longstaffe FJ, & Zazula GD (2010) Nursing, weaning, and tooth
797   development in woolly mammoths from Old Crow, Yukon, Canada: implications

798   for Pleistocene extinctions. *Palaeogeography, Palaeoclimatology, Palaeoecology*
799   298(3-4):257-270.

800 59.   Tacail T, Kovačiková L, Brůžek J, & Balter V (2017) Spatial distribution of trace
801   element Ca-normalized ratios in primary and permanent human tooth enamel.
802   *Science of the Total Environment* 603:308-318.

803 60.   Taylor D, Bligh P, & Duggan MH (1962) The absorption of calcium, strontium,
804   barium and radium from the gastrointestinal tract of the rat. *Biochemical Journal*
805   83(1):25.

806 61.   Gillespie B, d'Arcy H, Schwartz K, Bobo JK, & Foxman B (2006) Recall of age
807   of weaning and other breastfeeding variables. *International Breastfeeding Journal*
808   1:4-4.

809 62.   Hoppe KA, Koch PL, & Furutani TT (2003) Assessing the preservation of
810   biogenic strontium in fossil bones and tooth enamel. *International Journal of*
811   *Osteoarchaeology* 13(1-2):20-28.

812 63.   Hinz EA & Kohn MJ (2010) The effect of tissue structure and soil chemistry on
813   trace element uptake in fossils. *Geochimica et Cosmochimica Acta* 74(11):3213-
814   3231.

815 64.   Radosevich SC (1993) The Six Deadly Sins of Trace Element Analysis: A Case of
816   Wishful Thinking in Science. *Investigations of Ancient Human Tissue: Chemical*
817   *Analyses in Anthropology*, ed Sandford MK (Gordon and Breach), pp 269-332.

818 65.   Kohn MJ & Moses RJ (2013) Trace element diffusivities in bone rule out simple
819   diffusive uptake during fossilization but explain in vivo uptake and release.
820   *Proceedings of the National Academy of Sciences of the United States of America*
821   110(2):419-424.

822 66.   Reynard B & Balter V (2014) Trace elements and their isotopes in bones and
823   teeth: diet, environments, diagenesis, and dating of archeological and
824   paleontological samples. *Palaeogeography, Palaeoclimatology, Palaeoecology*
825   416:4-16.

826 67.   Millard AR & Hedges REM (1996) A diffusion-adsorption model of uranium
827   uptake by archaeological bone. *Geochimica et Cosmochimica Acta* 60(12):2139-
828   2152.

829 68.   Krestou A, Xenidis A, & Panias D (2004) Mechanism of aqueous uranium (VI)
830   uptake by hydroxyapatite. *Minerals Engineering* 17(3):373-381.

831 69.   Grün R, Aubert M, Joannes-Boyau R, & Moncel M-H (2008) High resolution
832   analysis of uranium and thorium concentration as well as U-series isotope
833   distributions in a Neanderthal tooth from Payre (Ardèche, France) using laser
834   ablation ICP-MS. *Geochimica et Cosmochimica Acta* 72(21):5278-5290.

835 70.   Trueman CN & Tuross N (2002) Trace elements in recent and fossil bone apatite.
836   *Reviews in Mineralogy and Geochemistry* 48(1):489-521.

837 71.   Turner-Walker G & Peacock EE (2008) Preliminary results of bone diagenesis in
838   Scandinavian bogs. *Palaeogeography, Palaeoclimatology, Palaeoecology* 266(3-
839   4):151-159.

840 72.   Kohn MJ, Morris J, and Olin P. (2013) Trace element concentrations in teeth–a
841   modern Idaho baseline with implications for archeometry, forensics, and
842   palaeontology. *Journal of Archaeological Science* 40(4):1689-1699.

843   73.   Ikem A, Nwankwoala A, Odueyungbo S, Nyavor K, & Egiebor N (2002) Levels
844   of 26 elements in infant formula from USA, UK, and Nigeria by microwave
845   digestion and ICP–OES. *Food Chemistry* 77(4):439-447.
846   74.   Bilandžić N*, et al.* (2015) Determination of macro-and microelements in cow,
847   goat, and human milk using inductively coupled plasma optical emission
848   spectrometry. *Spectroscopy Letters,* 48(9):677-684.
849   75.   Björklund KL*, et al.* (2012) Metals and trace element concentrations in breast
850   milk of first time healthy mothers: a biological monitoring study. *Environmental*
851   *Health* 11(1):92.
852   76.   Li C, Solomons NW, Scott ME, & Koski KG (2016) Minerals and trace elements
853   in human breast milk are associated with Guatemalan infant anthropometric
854   outcomes within the first 6 months. *The Journal of Nutrition* 146(10):2067-2074.
855   77.   Friel JK*, et al.* (1999) Elemental composition of human milk from mothers of
856   premature and full-term infants during the first 3 months of lactation. *Biological*
857   *Trace Element Research* 67(3):225-247.
858   78.   Cleveland W, Grosse E, & Shyu W (1992) Local regression models. In 'Statistical
859   Models in S'.(Eds JM Chambers, TJ Hastie) pp. 309–376. Chapman & Hall: New
860   York.
861